Molecular Origin of Gerstmann-Sträussler-Scheinker Syndrome: Insight from Computer Simulation of an Amyloidogenic Prion Peptide

Isabella Daidone,[†*] Alfredo Di Nola,[‡*] and Jeremy C. Smith[§]
[†]Department of Chemistry, Chemical Engineering and Materials, University of L'Aquila, L'Aquila, Italy; [‡]Department of Chemistry, University of Rome "La Sapienza", Rome, Italy; and [§]UT/ORNL Center for Molecular Biophysics, Oak Ridge National Laboratory, Oak Ridge, Tennesse

ABSTRACT Prion proteins become pathogenic through misfolding. Here, we characterize the folding of a peptide consisting of residues 109–122 of the Syrian hamster prion protein (the H1 peptide) and of a more amyloidogenic A117V point mutant that leads in humans to an inheritable form of the Gerstmann-Sträussler-Scheinker syndrome. Atomistic molecular dynamics simulations are performed for 2.5 μs. Both peptides lose their α-helical starting conformations and assume a β-hairpin that is structurally similar in both systems. In each simulation several unfolding/refolding events occur, leading to convergence of the thermodynamics of the conformational states to within 1 kJ/mol. The similar stability of the β-hairpin relative to the unfolded state is observed in the two peptides. However, substantial differences are found between the two unfolded states. A local minimum is found within the free energy unfolded basin of the A117V mutant populated by misfolded collapsed conformations of comparable stability to the β-hairpin state, consistent with increased amyloidogenicity. This population, in which V117 stabilizes a hydrophobic core, is absent in the wild-type peptide. These results are supported by simulations of oligomers showing a slightly higher stability of the associated structures and a lower barrier to association for the mutated peptide. Hence, a single point mutation carrying only two additional methyl groups is here shown to be responsible for rather dramatic differences of structuring within the unfolded (misfolded) state.

INTRODUCTION

Prion disorders are caused by a structural change of the cellular form of the prion protein (PrP^C) into an abnormal, infectious scrapie form (PrP^{SC}) (1,2), that accumulates in the brain as β-sheet-rich amyloid plaques (3). Several models for the mechanism of the amyloidogenic process have been proposed and all involve a conformational change in the protein that leads to the formation of soluble oligomers, the primary cytotoxic species in many cases, which eventually nucleate the growth of larger fibers (4–9).

Prion diseases can occur sporadically by unknown causes, by infection or in inherited forms. One of the inherited forms in humans, the Gerstmann-Sträussler-Scheinker syndrome, is associated with an alanine-to-valine (A117V) mutation. This mutation lies within a highly conserved region (10) corresponding to residues 109–122 of the prion sequence (the H1 peptide). The conformational change occurring within the H1 region has been suggested to be an early step in the conversion of PrP^C to PrP^{SC} (11–13), although the exact mechanism remains unclear. Furthermore, other PrP regions have been suggested to drive the pathogenic conformational change (14,15).

The experimental characterization of amyloidogenic proteins and peptides and their structural transitions is often hampered by their tendency to aggregate. However, useful information has been obtained by means of computer simulation (5,8,16–22). Homology modeling studies (23) led to the region corresponding to residues 109–122 in PrP^C being initially proposed to be α-helical. However, later in the NMR structure of PrP^C in solution the structure of this segment was found to be undefined (24). The isolated H1 peptide adopts a helical conformation in a water/2,2,2-trifluoroethanol mixture that is rapidly lost in pure water, in which the peptide forms β-sheet structure from which amyloid fibrils precipitate (11,25). The inclusion of the A117V point mutation was found to increase the toxicity of the peptide (26) and the β-sheet content in the fibrils (27). However, an explanation at the structural and thermodynamic levels of the higher amyloidogenicity caused by a single point mutation carrying only two additional methyl groups (alanine to valine) is still lacking.

In this study, we perform μs timescale atomistic molecular dynamics (MD) simulations in aqueous solution of the Syrian hamster H1 peptide and the mutated peptide carrying the A117V point mutation. Both peptides, initially modeled as a α-helix, spontaneously adopt a β-hairpin conformation that undergoes several unfolding/refolding transitions, to a degree permitting a thermodynamic and kinetic characterization of the folding/unfolding/misfolding process. Comparison of the two systems reveals significant differences consistent with the enhanced amyloidogenic character of the mutated peptide. Simulations of the early oligomerization process were also performed and show increased stability of the associated state and a decreased barrier to association for the mutant, consistent with the single-peptide results.

Submitted November 30, 2010, and accepted for publication April 25, 2011.

*Correspondence: daidone@caspur.it or dinola@caspur.it

Editor: Ruth Nussinov.

0006-3495/11/06/3000/8 $2.00

doi: 10.1016/j.bpj.2011.04.053

MATERIAL AND METHODS

Molecular dynamics simulation protocol

The explicit solvent simulations of the wild-type (WT) H1 peptide (MKHMAGAAAAGAVV) and of its A117V mutant (MKHMAGAAVA GAVV) were performed under the same physicochemical conditions with the same force field for the peptide, namely GROMOS96 (28), and for the solvent, namely the simple point charge model (29). The simulations were performed in the NVT ensemble with the isokinetic temperature coupling to keep the temperature constant at 300 K (30). For the oligomeric simulations (see below) a higher temperature of 400 K was used to enhance the configurational sampling. The bond lengths were fixed (31) and a time step of 2 fs was used for numerical integration of the equations of motion. The long-range electrostatic interactions were treated with the particle mesh Ewald method (32), with a real space cutoff of 0.9 nm. Coordinates were stored every 1 ps. The side chain protonation states reproduce a pH of ~7. The N- and C-termini were amidated and acetylated, respectively (11). For the monomeric simulations, one peptide molecule was placed in a periodic truncated octahedron large enough to contain $\approx$1.0 nm of water on all sides, and one negative counter ion (Cl^-) was added to neutralize the system. For the WT peptide 240 ns of MD simulation were performed starting from the α-helix conformation obtained in previous work (33), and 2260 ns starting from the β-hairpin conformation observed during the previous 240 ns simulation, using a new set of initial velocities, for a total simulation time of 2.5 μs. For the A117V mutant the same starting structures as for the WT were used and with Ala-117 mutated into a Val residue; 850 ns were performed starting from the α-helix and 1650 ns starting from the β-hairpin conformation, using a new set of initial velocities, for a total simulation time of 2.5 μs; concerning the choice of the starting configuration, a logical choice is a realistic, but non-beta initial structure, to possibly observe a transition into some β structure. Hence, rather than from a more unrealistic extended structure, the simulations were started from a α-helix conformation obtained in previous work in a 2,2,2-trifluoroethanol /water mixture (33).

For the oligomer simulations, four monomers with a starting β-hairpin conformation were placed in a periodic truncated octahedron large enough to contain $\approx$1.0 nm of water on all sides, and four negative counter ions (Cl^-) were added to neutralize the system. The four monomers were initially arranged in a plane with the turns pointing toward the center of an ideal circle, to maximize the distance between them while keeping the box a reasonable size. For both the WT and A117V tetramers the simulations were run for 300 ns.

Secondary structure definition

A robust parameter for identifying conformational transitions from the unfolded state to β-hairpin conformations is the R parameter (34), defined as follows:

$$R = \sum_{i=1}^{5} \frac{R_{i,N}}{R_i},$$

where $R_{i,N}$ is the ith interstrand C_α-C_α distance in the β-hairpin (native) structure and R_i is the same distance in the MD. The five interstrand C_α-C_α pairs in the H1 peptide hairpin are the following: M109-V121, K110-A120, H111-A118, M112-A117 (or V117), and A113-A116. A value of $R \approx 4.8$–5 indicates formation of the β-hairpin. A cut-off value of $R \geq 4.8$ was here used to define folded conformations (state f). To analyze the structural features of nonfolded conformations ($R < 4.8$), an RMSD (root mean-square deviation)-based clustering analysis (35) of those configurations with $R < 4.8$ was performed. Although for the WT peptide the unfolded structures do not possess persistent structural features, i.e., each cluster is populated by <5%, for the A117V mutant the highest populated cluster ($\approx$30% of the nonfolded conformations) does exhibit partial structuring, involving a β-bridge between H111 and V117 and with the side chain of V117 being buried, i.e., with a solvent accessible surface area ≤ 0.5 nm^2. Hence, for the WT all the nonfolded structures were classified as unfolded (u state), whereas in the case of the A117V mutant nonfolded conformations were themselves clustered into two states, i.e., a completely unfolded (state u) and misfolded (state m), the latter being the more populated.

Essential dynamics analysis

The principles of essential dynamics analysis are described in detail elsewhere (36,37). Briefly, the covariance matrix of positional fluctuations (C_α only) is constructed, from equilibrium MD trajectories and diagonalized. The corresponding eigenvectors are directions in configurational space and the eigenvalues indicate the mean-square fluctuations along these axes. The procedure corresponds to a linear multidimensional least squares fitting of a trajectory in configurational space. Sorting the eigenvectors by the size of the eigenvalues results in the division of the configurational space into a low-dimensional (essential) subspace in which most of the positional fluctuations are confined and a high-dimensional (near-constraints) subspace in which mostly small vibrations occur. The first essential eigenvector, ev 1, i.e., that with the largest eigenvalue, accounts for $\approx$45% of the overall positional fluctuations in both the WT and A117V mutant simulations and is here taken as the folding reaction coordinate (for the justification of this see the Results).

Free energy profile evaluation

To obtain the free energy along ev 1, the MD structures sampled every 1 ps were projected onto 80 bins dividing the overall accessible range. For each bin (i.e., for each position, q, along ev 1) the number of points was counted and the relative probability density, $\rho_{eq}(q)$, calculated together with the equilibrium fractions of folded, misfolded, and unfolded conformations. As the reference state, the bin with the highest probability density $\rho_{eq}(q_{ref})$, i.e., the bin corresponding to the overall free energy minimum, was chosen. The free energy profile was evaluated as

$$\Delta A(q) = -RT \ln \frac{\rho_{eq}(q)}{\rho_{eq}(q_{ref})}.$$

To check the effect of different grid spacings on the thermodynamic properties, the free energy profiles were constructed using different numbers of bins: 40, 50, 60, and 100. All the choices provided similar free energy profiles, the surface being slightly rougher with the higher (100 bins) number of bins than with the lower (40 bins).

RESULTS AND DISCUSSION

MD simulation of monomers

A structural, thermodynamic, and kinetic analysis of the folding-unfolding of the H1 peptide at room temperature, obtained using a long timescale (1 μs) atomistic MD simulation in explicit water, has been previously described (18,19,33). For this study an additional 2.5 μs simulation was performed, this time of the A117V mutated H1 peptide, under the same conditions. Furthermore, the WT H1 peptide simulation was extended to 2.5 μs.

In both simulations the peptide, initially modeled as a α-helix, preferentially adopts a β-hairpin conformation that undergoes several unfolding/refolding transitions. Representative structures of the observed β-hairpins and the

time evolution of the R parameter characterizing the secondary structural state of the peptides (see Methods), are shown in Fig. 1. The hairpin conformation is very similar for the two systems. The hairpin of the WT peptide, for which more detailed experimental data are available, is consistent with NMR chemical shifts (11) and with a low-resolution structure derived using x-ray diffraction (25). Comparing the solvent accessible surface area (SASA) of the folded hairpin structures ($R \geq 4.8$) shows that the only difference is in residue V117. The slight increase of ≈ 0.25 nm^2 in the SASA of the valine 117 of the mutated hairpin is due simply to the elongated side chain.

To characterize the folding/unfolding thermodynamics in the two systems, the free energy profiles of the WT and A117V mutated peptides along the first essential eigenvector (see Methods) were derived and are reported in Figs. 2 *A* and *B*, respectively. The WT peptide is characterized by a downhill, almost barrierless, profile. In contrast, the profile of the A11V mutant is double welled with a free energy barrier of $\approx$3–5 kJ/mol separating the two wells.

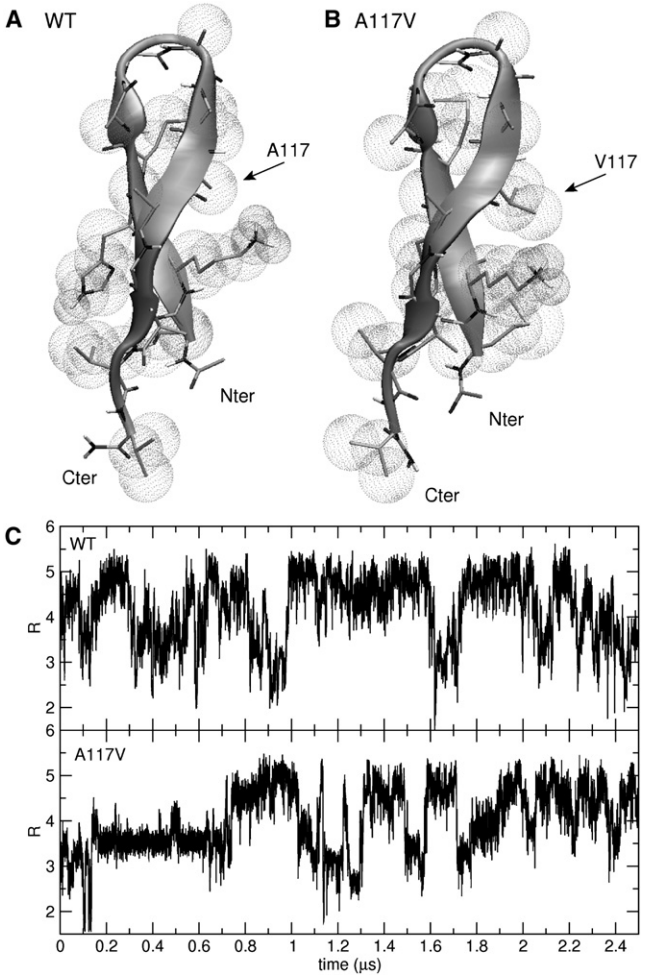

FIGURE 1 Representative fully folded β-hairpin structures observed (*A*) in the WT and (*B*) in the A117V simulations. (*C*) Time evolution of the R parameter for the WT (*top*) and A117V mutant (*bottom*) peptides.

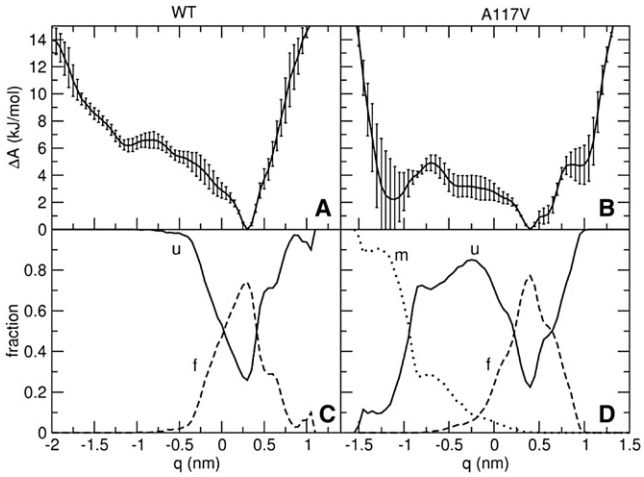

FIGURE 2 Free energy profile, $\Delta A(q)$, as a function of the position q along the first essential eigenvector for (*A*) the WT peptide and (*B*) the A117V mutant. Equilibrium fraction of folded, f, unfolded, u, and misfolded, m, conformations as a function of the position q along the first essential eigenvector for (*C*) the WT and (*D*) the A117V mutant. Error bars shown throughout the manuscript correspond to the standard error of the mean value of the corresponding property calculated over three subsets of the trajectory.

The equilibrium functions of the folded, f, unfolded, u, and misfolded, m, states (see Methods for the definitions) are shown as a function of the position q along the first essential eigenvector (ev 1) for the WT and mutated peptide in Fig. 2 *C* and *D*. For both peptides the folded β-hairpin structures form the major fraction at the free energy minimum (at $q \approx 0.3$ nm), whereas at the minimum the population of the unfolded state u drops to $\approx 20\%$. These results show that the first essential eigenvector is an appropriate reaction coordinate for distinguishing between folded and unfolded conditions.

In the case of the A117V mutant a local minimum is present in the unfolded basin (at $q \approx -1.2$ nm), which is absent in the WT. This local minimum is populated by a stable misfolded collapsed conformation, m. The corresponding equilibrium distribution as a function of q is shown in Fig. 2 *D*.

The structure of the misfolded collapsed conformation, m, is shown in Fig. 3 *A*. m is characterized by a β-bridge between H111 and V117 and β-bends between A118 and G119 and between A113 and A115. The side chain of V117 is oriented toward the C-terminal end of the peptide, forming a stable hydrophobic core. Comparison of the SASA in the f and m states (Fig. 3 *B*) shows, indeed, a smaller solvent-exposed surface area in the misfolded conformation. Hence, the two extra methyl groups are sufficient to drive the formation of a stable hydrophobic core that is not stably formed in the WT peptide.

To quantitatively compare the thermodynamics of the two systems, the stability of the unfolded state relative to that of the folded (and, when present, misfolded) state was

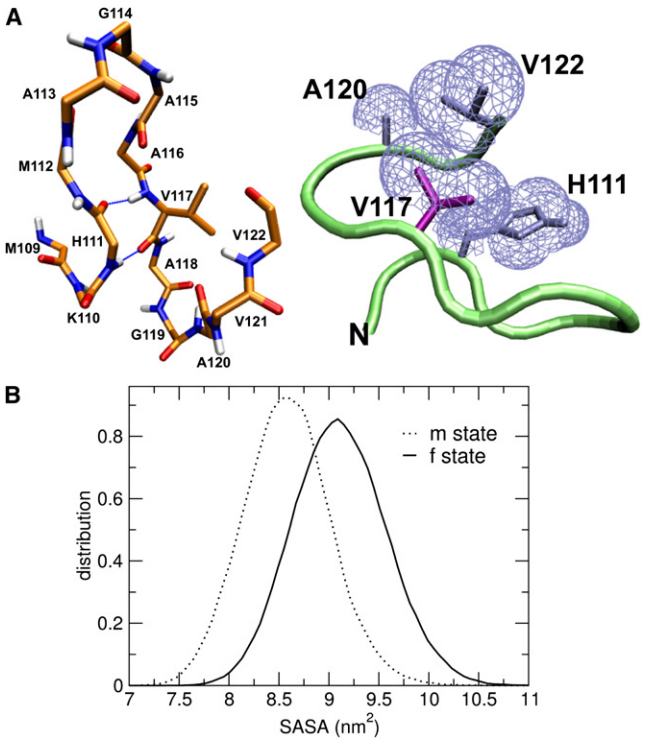

FIGURE 3 (*A*) Structure of the misfolded collapsed conformation from the A117V mutant MD simulations. Left: backbone conformation. Right: the side chains forming the hydrophobic core. (*B*) Distribution of the SASA of the conformations in the *f* and *m* states from the A117V mutant MD simulation.

calculated. Given thermodynamic equilibrium, at constant temperature and volume, the stability is given by the free energy difference between *u* and *f*(or *m*)

$$\Delta A_{u\rightarrow f(\text{or } m)} = -RT \ln \frac{p_{f(\text{or } m)}}{p_u},$$

where R is the ideal gas constant, T is the temperature, and $p_{f(\text{or } m)}$ and p_u are the probabilities of being in states *f*(or *m*) and *u*, respectively. Fig. 4 presents the sampling dependence of the free energy change estimate for the $u \rightarrow f$ transition for the WT and for the $u \rightarrow f$ and $u \rightarrow m$ transitions for the A117V peptide. In both simulations convergence of the free energy values is achieved within $\approx$2.5 μs, such that free energy changes associated with the conformational transitions are obtained to within 1.0 kJ/mol statistical accuracy. The free energy change for the $u \rightarrow f$ transition is similar in both systems ($\Delta A_{u \rightarrow f} \approx 2.8 \pm 1$ kJ/mol) corresponding to higher stability of the unfolded state relative to the β-hairpin. The 3 ± 1 kJ/mol values of $\Delta A_{u \rightarrow f}$ are consistent with experimental values ranging from ≈ -7 to $\approx$3.5 kJ/mol for various β peptides (38). The $u \rightarrow m$ free energy change in A117V is slightly higher than, but within the statistical noise of, the $u \rightarrow f$ free energy change ($\Delta A_{u \rightarrow m} \approx 3.4 \pm 1$ kJ/mol versus $\Delta A_{u \rightarrow f} \approx 2.8 \pm 1$ kJ/mol), and thus the folded and misfolded states are of comparable stability.

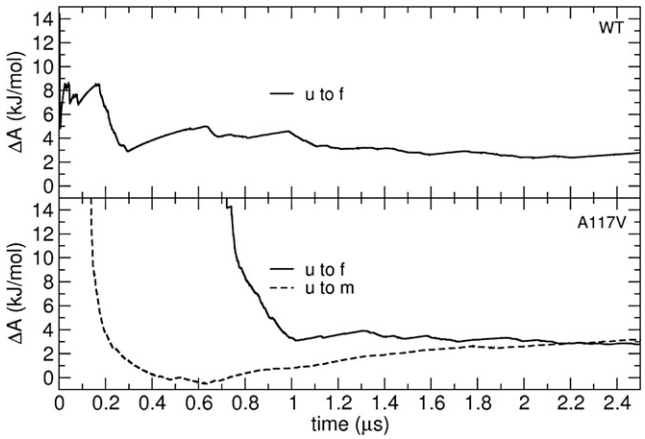

FIGURE 4 Convergence with time of the free energy change, $\Delta A_{u \rightarrow f}$, corresponding to the transition from the unfolded (*u*) to the folded (*f*) state from the WT (*top panel*) and A117V (*bottom panel*) simulations. For the A117V mutant, the free energy change upon misfolding, $\Delta A_{u \rightarrow m}$, is also shown. The final values at 2.5 μs are the equilibrium free energies and exhibit statistical accuracy within 1.0 kJ/mol. $\Delta A_{u \rightarrow f} \approx 2.8 \pm 1$ kJ/mol for the WT and $\Delta A_{u \rightarrow f} \approx 2.8 \pm 1$ kJ/mol, and $\Delta A_{u \rightarrow m} \approx 3.4 \pm 1$ kJ/mol for the A117V mutant.

Finally, the folding ($u \rightarrow f$) and unfolding ($f \rightarrow u$) kinetics were calculated. For the A117V mutant the misfolding $u \rightarrow m$ and $m \rightarrow u$ kinetics were also determined. The distributions of the mean first passage times for the different transitions are reported in Fig. 5. The corresponding mean transition times were determined by fitting the distributions with a biexponential function. This yielded for all possible transitions two time constants, one, τ_1, on the ps timescale (corresponding to relatively uninteresting fluctuations) and the second, τ_2, on the ns timescale (see Table 1). τ_2 for the folding ($u \rightarrow f$) and unfolding ($f \rightarrow u$) transitions are similar for the two peptides ($\tau_2 \approx$20–25 ns and $\tau_2 \approx 2$ ns, respectively), the unfolding transition thus being one order of magnitude faster than the folding transition. The $u \rightarrow m$ and $m \rightarrow u$ transitions, present only in the A117V mutant, have time constants of $\tau_2 \approx 42$ ns and $\tau_2 \approx 0.1$ ns, respectively. $u \rightarrow m$ is hence slower than $u \rightarrow f$ ($\approx$42 ns vs. $\approx$23 ns) and $m \rightarrow u$ is faster than $f \rightarrow u$ (1.8 ns vs. 0.1 ns). Direct transitions between *f* and *m* were never observed in the simulation.

MD simulation of oligomers

To study the initial stages of the oligomerization process, 300-ns-long MD simulations of four peptide monomers in aqueous solution were performed for the WT and the mutated peptide. For both systems during the simulations several association events on the nanosecond timescale occur, as shown by the time dependence of the total solvent accessible surface area (see Fig. 6 *A*). The free energy profiles of the WT and A117V mutated peptides as a function of the total SASA is reported in Fig. 6 *B* and clearly shows, for both systems, the presence of two well-separated

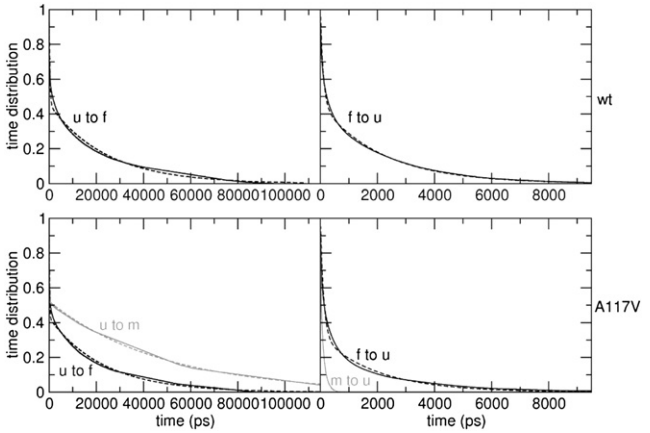

FIGURE 5 Distribution of the mean first passage times for the $u \rightarrow f$ and $f \rightarrow u$ transitions from the WT peptide (*top*) and the A117V mutant (*bottom*) simulations. For the A117V peptide the $u \rightarrow m$ and $m \rightarrow u$ distributions are also shown. The biexponential fits are shown with the dashed line.

minima, one at $\approx 38\ nm^2$ corresponding to aggregated configurations, and the other at ≈ 47–$60\ nm^2$, corresponding to dissociated configurations. Although the two profiles are very similar, they differ in both the relative stability of oligomeric structures with respect to dissociated conformations and the free energy barrier to association. The mutation has the effect of lowering by ≈ 1 kJ/mol the free energy of the oligomers relative to the dissociated structures and of reducing by ≈ 2 kJ/mol the barrier to association, from ≈ 7 kJ/mol to ≈ 5 kJ/mol.

A structural analysis revealed that the observed oligomers contain very heterogeneous β-sheet structures, i.e., they always involve different parts of different monomers. Some of the oligomers display β-barrel conformations, in agreement with previous studies showing transient β-barrel assemblies in the early aggregation steps of amyloid-forming systems (39). On average, the sheet structures are characterized by ≈ 15 interpeptide hydrogen bonds and

TABLE 1 Folding, misfolding, and unfolding time constants

	$u \rightarrow f$	$u \rightarrow m$	$f \rightarrow u$	$m \rightarrow u$
WT				
τ_1	313 (23) ps	–	102 (19) ps	–
K_1	55%	–	55%	–
τ_2	24.0 (5.2) ns	–	2.2 (0.3) ns	–
K_2	45%	–	45%	–
A117V				
τ_1	176 (32) ps	40 (12) ps	113 (21) ps	20 (8) ps
K_1	57%	48%	68%	40%
τ_2	23.1 (5.8) ns	42.3 (9.1) ns	1.8 (0.2) ns	0.1 (0.03) ns
K_2	43%	52%	32%	60%

Transition time distributions (see Fig. 5) were fitted using a biexponential function: $K_1 e^{-(t/\tau_1)} + K_2 e^{-(t/\tau_2)}$. The τ_1 and τ_2 are the fast and slow time constants, respectively, and the K_1 and K_2 the corresponding amplitudes. Errors shown throughout the manuscript, here reported in parenthesis, correspond to the standard error of the mean value of the corresponding property calculated over three subsets of the trajectory.

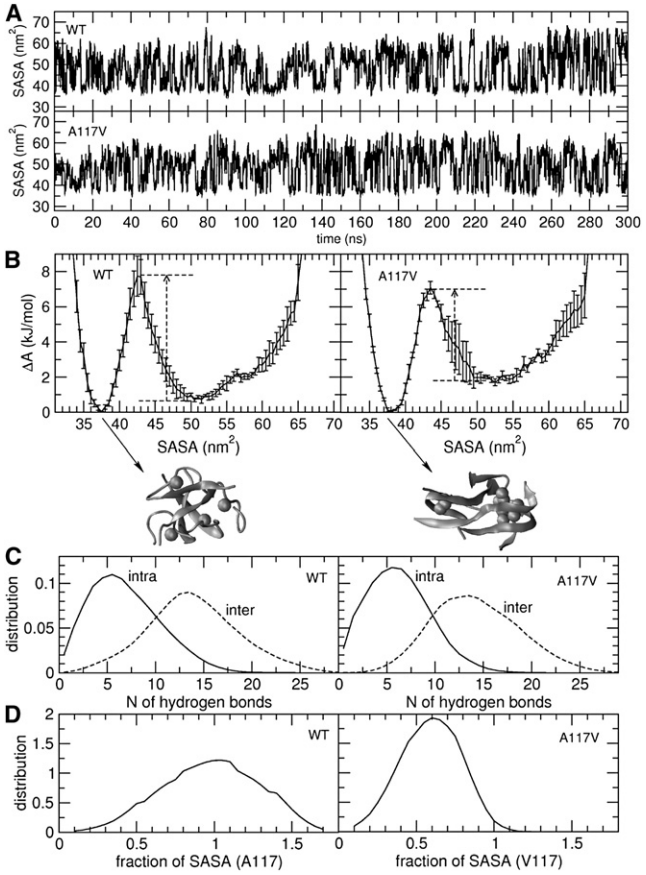

FIGURE 6 Time evolution of the total SASA (*A*) and corresponding free energy profile, ΔA, as a function of the total SASA (*B*) for the oligomeric simulation of the WT and A117V mutant peptides. Representative β-sheet oligomeric structures are also given. (*C*) Distribution of the number of intrapeptide and interpeptide hydrogen bonds in the simulation of the oligomeric WT and A117V mutant peptides. (*D*) Distribution of the SASA fraction of the side chain of residue A117 (for the WT) and V117 (for the mutant) in the simulation of the oligomeric WT and A117V mutant peptides. The fraction is given with respect to the corresponding SASA in the starting configuration.

≈ 5 intrapeptide hydrogen bonds (see Fig. 6 *C*). The misfolded conformation sampled by the isolated A117V mutant was never observed in the oligomeric simulations. Hence, the oligomerization process involves mainly partly extended strands, rather than the hairpin conformation used as the starting structure or the misfolded conformation mentioned previously. These data suggest that partly extended, unfolded structures might be precursors of the oligomerization process (see scheme in Fig. 7), in accord with the experimental evidence that in the intact PrP^C protein residues 109–122 (i.e., the sequence corresponding to the H1 peptide) is structurally disordered (24).

Finally, the solvent accessibility of the side chain of residue 117 in the WT and mutant oligomeric simulations was investigated. The SASA of A117 (in the WT) and V117 (in the mutant) has been divided by the corresponding SASA in the starting conformation formed by the four

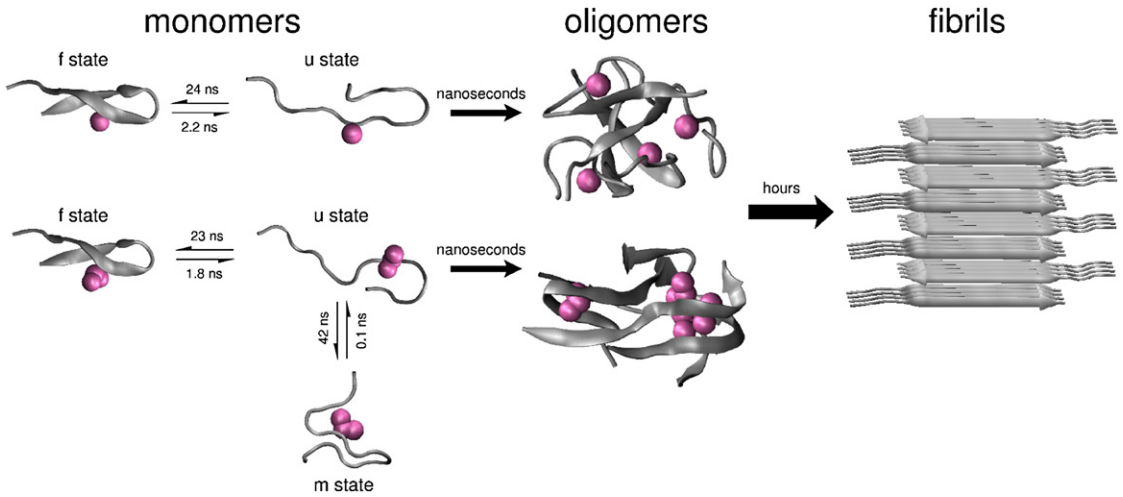

FIGURE 7 Schematic diagram of the folding/misfolding/oligomerization process for the WT (*top*) and A117V mutant (*bottom*) peptides. The side chain of residue 117 is highlighted. In the monomeric state, the mean first passage times associated with the different transitions are shown. It can be seen that the main difference is that, although V117 dives the formation of a misfolded monomeric conformation in the mutant simulation, such a misfolded state is not present in the WT peptide. When more monomers are considered in the same solution, formation of oligomers possessing some β-sheet structure occurs in both systems on the nanosecond timescale. Again, in contrast to the WT system, in the mutant oligomers the V117 side chains tend to participate in interpeptide hydrophobic cores. Precursors of the oligomerization process are mainly partly extended, unfolded peptide units in both systems. The formation of oligomers will eventually nucleate the growth of large fibrils on much longer timescales (at least hours). Nucleation of mature fibers was not studied in this work.

hairpin monomers to provide information on the fraction of surface that becomes buried upon clustering (see Fig. 6 *D*). It can be seen that while for the WT system the A117 side chain remains rather exposed to the solvent (the distribution of the SASA fraction being peaked at ≈ 1), the SASA of the V117 side chain of the mutant reduces to $\approx 60\%$ of the corresponding SASA in the initial configuration. Hence, upon clustering of the mutant, the side chains of V117 become involved in hydrophobic cores, in contrast to the A117 side chains of the WT that remain mainly solvent exposed (see scheme in Fig. 7).

It has been suggested that in the stable, mature fibers of both the WT and mutated H1 peptide, the monomers are aligned in an antiparallel fashion with only residues 112–122 (the hydrophobic core) participating to the β-sheets (40,41) (see scheme in Fig. 7). However, the observation of the nucleation of a stable core acting as precursor of the fibrillization process is beyond the scope of this work and would require much longer trajectories or coarse-grained simulations (20–22,42–44).

CONCLUSIONS

There is a considerable interest in understanding the molecular mechanisms of misfolding in prion and other amyloid diseases, such as Alzheimer's, Huntington's, and Parkinson's (1,45–47) and there is hope that this understanding might eventually lead to new therapies for these illnesses. Prion diseases can occur in inherited forms characterized by an early onset of the disease and aggravated severity. The majority of the familial forms originate from single-point mutations.

In this work, the effect of the Gerstmann-Sträussler-Scheinker alanine-to-valine mutation on the structure, thermodynamics, and kinetics of the H1 prion peptide in aqueous solution is studied by means of long (2.5 μs) MD simulations in explicit water. Both the WT and A117V peptides, initially modeled as a α-helix, spontaneously form a similar β-hairpin conformation, in which the side chain of residue 117 is exposed to the solvent, the only slight difference being an increase of ≈ 0.25 nm^2 of the exposed surface area of residue 117 in the A117V peptide. In contrast to the folded state, dramatic effects are seen in the unfolded states of the two peptides. A stable misfolded conformation populates a local minimum in the unfolded basin of the mutated A117V peptide, in which the residue V117 is buried in a hydrophobic core. No stable misfolded hydrophobic core is present in the WT.

The higher tendency observed for the isolated A117V peptide to form misfolded, compact conformations is consistent with the higher aggregation propensity experimentally observed for the mutated peptide. Simulation of the initial oligomerization process of four peptide monomers for the WT and mutated peptides qualitatively confirms this hypothesis, showing (within the 300 ns simulation time) slightly higher stability of the oligomeric structures and a lower barrier to association for the mutated peptide relative to the WT system. No experimental data exist on the early oligomerization stages in the two systems. However, a similar effect, supporting our results, was observed in the case of an Alzheimer's amyloid β-peptide for which the E22Q mutation was found to lower the barrier for monomer deposition onto a pre-formed fibril (8).

In the intact PrP^C protein the A117V mutation lies within a highly conserved region that is structurally disordered (24). This suggests that the conformational change within this region, that is thought to be an early step in the conversion of PrP^C to PrP^{SC} (11,12), takes place from an unfolded conformation rather than from a folded structure. In accord with these data on the intact PrP^C, partly extended configurations are found here as the dominant components of the oligomers. Hence, the structural and thermodynamic differences observed in the unfolded state of the WT and mutant systems might explain the higher misfolding propensity induced by the mutation.

Concerning the kinetics, the folding transition (from unfolded to β-hairpin conformations) is shown to be on the order of tens of nanoseconds in both systems. However, in the A117V mutant an additional transition occurs on the ns timescale, corresponding to the misfolding transition from the unfolded to the collapsed, misfolded state (see scheme in Fig. 7). Folding times of the order of tens of nanoseconds are faster than the known folding times for non-amyloidogenic β-peptides (the fastest being $\approx$260 ns (38,48,49)) and of the same order of magnitude as for α-helices. Although this may be due in part to limitations arising from the empirical force fields used, it is likely to also reflect the amyloidogenic nature of the peptides studied (11) and is consistent with the very high alanine content reducing the entropic costs for the β-hairpin formation (48) (similarly to alanine-rich helices).

Finally, and more generally, the present results highlight the need, when characterizing the effects of mutations on peptide and protein stability, to consider structural changes occurring in the unfolded state (50–54). Focusing solely on changes occurring in the native state can miss effects crucial to the folding/misfolding process.

The authors acknowledge Eva Kowalinski for helpful discussions. A.D.N. acknowledges the University of Rome "La Sapienza" for financial support with the project "Morfogenesi molecolare, un approccio multidisciplinare per lo studio del folding e misfolding delle proteine" and CASPUR (Consorzio Interuniversitario per le Applicazioni di Supercalcolo Per Universitá e Ricerca) for the use of its computational facilities. J.C.S. acknowledges funding through a Department of Energy Laboratory-Directed Research and Development Award to Oak Ridge National Laboratory.

REFERENCES

1. Prusiner, S. B. 1991. Molecular biology of prion diseases. *Science.* 252:1515–1522.
2. Kelly, J. W. 1997. Amyloid fibril formation and protein misassembly: a structural quest for insights into amyloid and prion diseases. *Structure.* 5:595–600.
3. Borchelt, D. R., M. Scott, …, S. B. Prusiner. 1990. Scrapie and cellular prion proteins differ in their kinetics of synthesis and topology in cultured cells. *J. Cell Biol.* 110:743–752.
4. Pan, K. M., M. Baldwin, J. Nguyen, M. Gasset, A. Serban, D. Groth, I. Mehlhorn, Z. Huang, R. J. Fletterick, F. E. Cohen…, 1993. Conversion of α-helices into β-sheets features in the formation of the scrapie prion proteins. *Proc. Natl. Acad. Sci. USA.* 90:10962–10966.
5. Ma, B. Y., and R. Nussinov. 2002. Stabilities and conformations of Alzheimer's β -amyloid peptide oligomers (Abeta 16-22, Abeta 16-35, and Abeta 10-35): sequence effects. *Proc. Natl. Acad. Sci. USA.* 99:14126–14131.
6. Caughey, B., and P. T. Lansbury. 2003. Protofibrils, pores, fibrils, and neurodegeneration: separating the responsible protein aggregates from the innocent bystanders. *Annu. Rev. Neurosci.* 26:267–298.
7. Kayed, R., E. Head, …, C. G. Glabe. 2003. Common structure of soluble amyloid oligomers implies common mechanism of pathogenesis. *Science.* 300:486–489.
8. Baumketner, A., M. G. Krone, and J. E. Shea. 2008. Role of the familial Dutch mutation E22Q in the folding and aggregation of the 15-28 fragment of the Alzheimer amyloid-beta protein. *Proc. Natl. Acad. Sci. USA.* 105:6027–6032.
9. Walsh, P., P. Neudecker, and S. Sharpe. 2010. Structural properties and dynamic behavior of nonfibrillar oligomers formed by PrP(106-126). *J. Am. Chem. Soc.* 132:7684–7695.
10. Schätzl, H. M., M. Da Costa, …, S. B. Prusiner. 1995. Prion protein gene variation among primates. *J. Mol. Biol.* 245:362–374.
11. Nguyen, J., M. A. Baldwin, …, S. B. Prusiner. 1995. Prion protein peptides induce α-helix to β-sheet conformational transitions. *Biochemistry.* 34:4186–4192.
12. Kazmirski, S. L., D. O. V. Alonso, …, V. Daggett. 1995. Theoretical studies of sequence effects on the conformational properties of a fragment of the prion protein: implications for scrapie formation. *Chem. Biol.* 2:305–315.
13. Okimoto, N., K. Yamanaka, …, T. Hoshino. 2002. Computational studies on prion proteins: effect of Ala(117)—>Val mutation. *Biophys. J.* 82:2746–2757.
14. Chakroun, N., S. Prigent, …, H. Rezaei. 2010. The oligomerization properties of prion protein are restricted to the H2H3 domain. *FASEB J.* 24:3222–3231.
15. Hosszu, L. L., M. H. Tattum, …, A. R. Clarke. 2010. The H187R mutation of the human prion protein induces conversion of recombinant prion protein to the PrP(Sc)-like form. *Biochemistry.* 49:8729–8738.
16. Kuwata, K., T. Matumoto, …, H. Roder. 2003. NMR-detected hydrogen exchange and molecular dynamics simulations provide structural insight into fibril formation of prion protein fragment 106-126. *Proc. Natl. Acad. Sci. USA.* 100:14790–14795.
17. Ding, F., J. J. LaRocque, and N. V. Dokholyan. 2005. Direct observation of protein folding, aggregation, and a prion-like conformational conversion. *J. Biol. Chem.* 280:40235–40240.
18. Daidone, I., A. Amadei, and A. Di Nola. 2005. Thermodynamic and kinetic characterization of a β-hairpin peptide in solution: an extended phase space sampling by molecular dynamics simulations in explicit water. *Proteins.* 59:510–518.
19. Daidone, I., M. D'Abramo, …, A. Amadei. 2005. Theoretical characterization of α-helix and β-hairpin folding kinetics. *J. Am. Chem. Soc.* 127:14825–14832.
20. Fawzi, N. L., E. H. Yap, …, T. Head-Gordon. 2008. Contrasting disease and nondisease protein aggregation by molecular simulation. *Acc. Chem. Res.* 41:1037–1047.
21. Bellesia, G., and J. E. Shea. 2009. Diversity of kinetic pathways in amyloid fibril formation. *J. Chem. Phys.* 131:111102.
22. Rojas, A., A. Liwo, …, H. A. Scheraga. 2010. Mechanism of fiber assembly: treatment of Aβ peptide aggregation with a coarse-grained united-residue force field. *J. Mol. Biol.* 404:537–552.
23. Huang, Z., J. M. Gabriel, …, F. E. Cohen. 1994. Proposed three-dimensional structure for the cellular prion protein. *Proc. Natl. Acad. Sci. USA.* 91:7139–7143.
24. James, T. L., H. Liu, …, F. E. Cohen. 1997. Solution structure of a 142-residue recombinant prion protein corresponding to the infectious fragment of the scrapie isoform. *Proc. Natl. Acad. Sci. USA.* 94:10086–10091.

25. Inouye, H., and D. A. Kirschner. 1998. Polypeptide chain folding in the hydrophobic core of hamster scrapie prion: analysis by x-ray diffraction. *J. Struct. Biol.* 122:247–255.

26. Brown, D. R. 2000. Altered toxicity of the prion protein peptide PrP106-126 carrying the Ala(117)—>Val mutation. *Biochem. J.* 346:785–791.

27. Petty, S. A., T. Adalsteinsson, and S. M. Decatur. 2005. Correlations among morphology, beta-sheet stability, and molecular structure in prion peptide aggregates. *Biochemistry.* 44:4720–4726.

28. van Gunsteren, W. F., S. R. Billeter, …, I. G. Tironi. 1996. Biomolecular Simulation: The GROMOS96 Manual and User Guide. Hochschulverlag AG an der ETH Zürich, Zürich.

29. Berendsen, H. J. C., J. R. Grigera, and T. P. Straatsma. 1987. The missing term in effective pair potentials. *J. Phys. Chem.* 91:6269–6271.

30. Brown, D., and J. H. R. Clarke. 1984. A comparison of constant energy, constant temperature, and constant pressure ensembles in molecular dynamics simulations of atomic liquids. *Mol. Phys.* 51:1243–1252.

31. Hess, B., H. Bekker, …, J. G. E. M. Fraaije. 1997. LINCS: A linear constraint solver for molecular simulations. *J. Comput. Chem.* 18:1463–1472.

32. Darden, T., D. York, and L. Pedersen. 1993. Particle mesh Ewald: an N-log(N) method for Ewald sums in large systems. *J. Chem. Phys.* 98:10089–10092.

33. Daidone, I., F. Simona, …, A. Di Nola. 2004. β-hairpin conformation of fibrillogenic peptides: structure and α-β transition mechanism revealed by molecular dynamics simulations. *Proteins.* 57:198–204.

34. Yang, S., J. N. Onuchic, …, H. Levine. 2007. Folding time predictions from all-atom replica exchange simulations. *J. Mol. Biol.* 372:756–763.

35. Daura, X., K. Gademann, …, A. E. Mark. 1999. Peptide folding: when simulation meets experiment. *Angew. Chem. Int. Ed.* 38:236–240.

36. Amadei, A., A. B. M. Linssen, and H. J. C. Berendsen. 1993. Essential dynamics of proteins. *Proteins.* 17:412–425.

37. de Groot, B. L., A. Amadei, …, H. J. Berendsen. 1996. An extended sampling of the configurational space of HPr from *E. coli*. *Proteins.* 26:314–322.

38. Muñoz, V., R. Ghirlando, …, W. A. Eaton. 2006. Folding and aggregation kinetics of a β-hairpin. *Biochemistry.* 45:7023–7035.

39. De Simone, A., and P. Derreumaux. 2010. Low molecular weight oligomers of amyloid peptides display beta-barrel conformations: a replica exchange molecular dynamics study in explicit solvent. *J. Chem. Phys.* 132:165103.

40. Silva, R. A., W. Barber-Armstrong, and S. M. Decatur. 2003. The organization and assembly of a β-sheet formed by a prion peptide in solution: an isotope-edited FTIR study. *J. Am. Chem. Soc.* 125:13674–13675.

41. Lee, S. W., Y. Mou, …, J. C. Chan. 2008. Steric zipper of the amyloid fibrils formed by residues 109-122 of the Syrian hamster prion protein. *J. Mol. Biol.* 378:1142–1154.

42. Pellarin, R., E. Guarnera, and A. Caflisch. 2007. Pathways and intermediates of amyloid fibril formation. *J. Mol. Biol.* 374:917–924.

43. Chebaro, Y., N. Mousseau, and P. Derreumaux. 2009. Structures and thermodynamics of Alzheimer's amyloid-β Abeta(16-35) monomer and dimer by replica exchange molecular dynamics simulations: implication for full-length Abeta fibrillation. *J. Phys. Chem. B.* 113:7668–7675.

44. Urbanc, B., M. Betnel, …, D. B. Teplow. 2010. Elucidation of amyloid β-protein oligomerization mechanisms: discrete molecular dynamics study. *J. Am. Chem. Soc.* 132:4266–4280.

45. Scherzinger, E., R. Lurz, …, E. E. Wanker. 1997. Huntingtin-encoded polyglutamine expansions form amyloid-like protein aggregates in vitro and in vivo. *Cell.* 90:549–558.

46. Dobson, C. M. 1999. Protein misfolding, evolution and disease. *Trends Biochem. Sci.* 24:329–332.

47. Aguzzi, A., and C. Haass. 2003. Games played by rogue proteins in prion disorders and Alzheimer's disease. *Science.* 302:814–818.

48. Xu, Y., R. Oyola, and F. Gai. 2003. Infrared study of the stability and folding kinetics of a 15-residue β-hairpin. *J. Am. Chem. Soc.* 125:15388–15394.

49. Xu, Y., P. Purkayastha, and F. Gai. 2006. Nanosecond folding dynamics of a three-stranded beta-sheet. *J. Am. Chem. Soc.* 128:15836–15842.

50. Lapidus, L. J., W. A. Eaton, and J. Hofrichter. 2000. Measuring the rate of intramolecular contact formation in polypeptides. *Proc. Natl. Acad. Sci. USA.* 97:7220–7225.

51. Baldwin, R. L. 2002. Making a network of hydrophobic clusters. *Science.* 295:1657–1658.

52. Lei, H., and P. E. Smith. 2003. The role of the unfolded state in hairpin stability. *Biophys. J.* 85:3513–3520.

53. Merchant, K. A., R. B. Best, …, W. A. Eaton. 2007. Characterizing the unfolded states of proteins using single-molecule FRET spectroscopy and molecular simulations. *Proc. Natl. Acad. Sci. USA.* 104:1528–1533.

54. Hoffmann, A., A. Kane, …, B. Schuler. 2007. Mapping protein collapse with single-molecule fluorescence and kinetic synchrotron radiation circular dichroism spectroscopy. *Proc. Natl. Acad. Sci. USA.* 104:105–110.